Research Article
doi.org/10.1002/batt.202200045

Chemistry Europe
European Chemical Societies Publishing

www.batteries-supercaps.org

Impact of Degree of Graphitization, Surface Properties and Particle Size Distribution on Electrochemical Performance of Carbon Anodes for Potassium-Ion Batteries

Jens M. Wrogemann,*[a] Olga Fromm,[a] Fabian Deckwirth,[b] Kolja Beltrop,[a, c] Andreas Heckmann,[a] Martin Winter,[a, b] and Tobias Placke*[a]

Carbons are considered as anode active materials in potassium-ion batteries (PIBs). Here, the correlation between material properties of disordered (non-graphitic) and ordered graphitic carbons and their electrochemical performance in carbon||K metal cells is evaluated. First, carbons obtained from heat treatment of petroleum coke at temperatures from 800 to 2800 °C are analyzed regarding their microstructure and surface properties. Electrochemical performance metrics for K^+ ion storage like specific capacity and Coulombic efficiency (C_{Eff}) are correlated with surface area, non-basal planes and microstructure properties, and compared to Li^+ ion storage. For disordered carbons, the specific capacity can be clearly correlated with the defect surface area. For highly ordered graphitic carbons, the degree of graphitization strongly determines the specific capacity. The initial C_{Eff} of graphitic carbons shows a strong correlation with basal and non-basal planes. Second, kinetic limitations of ordered graphitic carbons are re-evaluated by analyzing commercial graphites regarding particle size and surface properties. A clear correlation between particle size, surface area and well-known challenges of graphitic carbons in terms of low-rate capability and voltage hysteresis is observed. This work emphasizes the importance of bulk and surface material properties for K^+ ion storage and gives important insights for future particle design of promising carbon anodes for PIB cells.

Introduction

In the past decades, the demand on electrochemical energy storage (EES) technologies for portable electronics, electric vehicles (EVs) as well as for stationary grid storage has grown rapidly. Especially for portable devices and EVs, lithium ion batteries (LIBs) are considered as state-of-the-art battery technology due to a high volumetric and gravimetric energy densities, high power density and energy efficiency as well as long cycle life.[1] However, for stationary grid storage and larger applications, low acquisition and operating costs are a dominating factor and are required to compete with other EES technologies.[2] In terms of LIBs, lithium has been classified as critical raw material within the European Union due to the limited abundance of lithium resources and locally restricted occurrences since 2017,[3] which among others are and will be the main factors for increased costs today and in the future.[4] Therefore, various "post lithium (ion) batteries" like sodium-ion or potassium-ion batteries (SIBs/PIBs)[5] and multivalent-ion technologies (Mg,[6] Ca[7]) attract an increased attention over the last years. Due to the high abundance and expected lower raw material costs especially the familiar SIBs and PIBs were discussed as promising alternatives.[5a,8] However, to compete with LIBs in terms of costs, an increase in energy density based on optimization of active materials for both technologies is still required.

SIBs and PIBs are based on the same ion-transfer (rocking-chair) principle like LIBs, but there are notable differences strongly influenced by the (electro)chemical properties of the respective alkali ion. This is mainly caused by differing ionic radii (K^+: 1.38 Å; Na^+: 1.02 Å; Li^+: 0.76 Å) and atomic masses (K^+: 39.10; Na^+: 22.9; Li^+: 6.94) for the same charge.[9] As a result, K^+ ions show a weaker Lewis acidity than Li^+ and Na^+ ions, leading to a higher electrolyte conductivity of solvated K^+ ions due to a smaller solvation shell.[10] In common organic carbonate solvent electrolytes, like propylene carbonate or a mixture of ethylene carbonate and diethyl carbonate, the redox couple K|K^+ shows also even lower operating potentials than Li|Li^+ and Na|Na^+.[11] In addition, binary graphite intercalation compounds (GICs) can be formed electrochemically up to maximum stoichiometries of LiC_6[12] and KC_8,[13] whereas Na^+ intercalation is limited to NaC_{64}[14] or forms co-intercalated

[a] J. M. Wrogemann, Dr. O. Fromm, Dr. K. Beltrop, Dr. A. Heckmann, Prof. M. Winter0000-0003-4176-5811, Dr. T. Placke
University of Münster
MEET Battery Research Center
Corrensstraße 46, 48149 Münster, Germany
E-mail: jwrogemann@uni-muenster.de
tobias.placke@uni-muenster.de
Homepage: 0000-0003-4176-5811
[b] F. Deckwirth, Prof. M. Winter0000-0003-4176-5811
Helmholtz Institute Münster, IEK-12
Forschungszentrum Jülich GmbH
Corrensstraße 46, 48149 Münster, Germany
[c] Dr. K. Beltrop
E-Lyte Innovations GmbH
Mendelstraße 11, 48149 Münster, Germany

Supporting information for this article is available on the WWW under https://doi.org/10.1002/batt.202200045

ternary species based on ether-based solvents showing increased capacity.[15] Overall, PIBs could exhibit some promising benefits over SIBs for stationary EES applications in future, even though a strong optimization of active materials or even new materials are still required to really take advantage of potential benefits and to overcome assumed stronger volume expansion.[8a,16]

With regard to negative electrodes (anodes), various materials like insertion-/intercalation-type carbon materials (e.g., soft carbon,[17] hard carbon,[18] graphite,[19] carbon nanostructures,[20] doped carbon structures[21]), alloying-type materials (e.g., P,[22] Sb,[23]), and conversion-type materials (e.g., metal sulfides,[24] metal oxides[25]) have been studied intensively for reversible K^+ ion storage.[8a] However, due to their decent capacity, high abundance, high electronic conductivity, low cost and well-known processability, non-graphitic carbonaceous materials like hard (non-graphitizable) carbons, soft (graphitizable) carbons and especially graphite are considered as most suitable anode materials for a possible future industrial application. All three types of carbon anodes were already investigated for K^+ ion storage and show similar specific capacities between $\approx$200–270 mAh g^{-1}.[17b,19b,26] Among them, hard and soft carbons show a benefit in terms of improved rate capability due to the fast storage mechanism of K^+ ions, called adsorption, which is similar to Li^+ ion storage.[17b,26] Hard carbons are dominated by highly disordered stacked carbon units showing a high micro porosity. Based on the adsorption storage mechanism, especially hard carbons are assumed to show a reduced volume expansion caused by their porous structure and K^+ ion adsorption in nano-pores.[26a,27] However, due to the porous structure they also suffer from a low initial Coulombic efficiency (C_{Eff}), lower tap density and from a reduced volumetric electrode capacity.[26a] With regard to processability and costs, most of the hard carbon precursors show a lower carbon yield during synthesis compared to those of soft carbons.[28] Soft carbons are graphitizable disordered carbons consisting of small graphitic domains, which are weakly cross-linked. By thermal heat treatment the ordering of these domains is increased and more or less well-defined graphitic structures are formed.[28,29] Graphite itself also shows promising characteristics as anode material for K^+ ion storage due to the low operating potential and a moderate theoretical capacity of 279 mAh g^{-1}.[19b] However, graphite suffers from larger volume expansion and lower kinetics than soft carbon.[30] Soft carbons represent an interesting material class for K^+ ion storage due to their possibility to balance the advantages and disadvantages of adsorption and intercalation mechanisms. The stepwise heat treatment of soft carbon precursors allows to investigate the impact of different parameters on the electrochemical properties from highly disordered soft carbon to well-ordered graphite. The number of systematic studies about the correlation of the heat treatment temperature (HTT) of soft carbons and their electrochemical properties for K^+ ion storage is rare. Lin et al. used polyacrylonitrile-derived carbon nanofiber films as model material to investigate K^+ ion storage at three different carbonizing temperatures (650 °C, 1250 °C, 2800 °C) with regard to their different carbon microstructure.[31] Utilizing mesophase pitch carbon as commercial precursor, Tan et al. studied stepwise synthesized soft carbons (800–2800 °C) and characterized the storage mechanism systematically via in-situ Raman spectroscopy, recently.[30a] Both studies showed that a disordered microstructure is present at lower HTT, which leads to a fast K^+ adsorption mechanism, whereas a well-ordered structure at higher HTT is dominated by an intercalation-type K^+ ion storage suffering from low kinetics. However, it is well-known from LIBs, that not only the carbon microstructure influences the electrochemical properties of carbon anodes.[32] Also surface properties, like defect surface area and non-basal planes determine key performance indicators (KPIs) like specific capacity and C_{Eff} for reversible cation storage.[28,32a,b] Furthermore, the particle size, especially of graphite anodes, can also have a huge impact on the rate capability.[33] To the best of our knowledge, these important characteristics of carbonaceous anodes have not been systematically addressed for K^+ ion storage so far.

In this study, petroleum coke, an industrially used precursor for soft carbon and artificial/synthetic graphite, is stepwise heat-treated from 800–2800 °C and characterized as electrode material for K^+ ion storage. Surface properties and the degree of graphitization are correlated to different electrochemical performance indicators and the results are compared to data of Li^+ ion storage.[28] In a second part, commercial graphites with different particle sizes are characterized electrochemically, demonstrating a strong correlation of particle size, voltage hysteresis and rate capability for K^+ ion storage.

Experimental Section

Material synthesis

For the preparation of various carbonaceous anode active materials, petroleum coke (PET Coke 200, 200 mesh; *CGC Klein Carbon Graphite Consulting*) was used and prepared according to the previous publication.[28] In short, the precursor was first carbonized in a temperature range between 800 °C and 1000 °C under argon (Ar) atmosphere in a Nabertherm oven RS 80/75013 (*Nabertherm GmbH*). After grinding and sieving to a grain size of $<$ 75 µm the achieved materials were either used for electrode preparation or further heat treatment procedures ($>$1000 °C). Heat treatment in the temperature range between 1100 °C and 2100 °C was performed under Ar atmosphere to carbonize and/or graphitize the carbonized precursors by using a high temperature chamber furnace HTK 25 (*Carbolite Gero GmbH & Co.KG*), whereas for preparation at temperatures $>$2100 °C a LHTG 200–300/30-2G-oven (*Carbolite Gero GmbH & Co. KG*) was utilized. The target temperatures were achieved within 10 h and were held for additional 10 h.[28] Commercial synthetic graphite materials, named KS4, KS10, KS15, KS25, KS44 and SFG 44 (*Imerys Graphite & Carbon*), were used in the second part of the study to investigate the impact of particle size distribution on K^+ ion storage.

Physical characterization of carbonaceous materials

A Carl Zeiss AURIGA scanning electron microscope (*Carl Zeiss Microscopy GmbH*) was used at a nominal acceleration voltage of 3 keV to observe the morphology of the precursor as well as of the prepared and investigated materials.

For insights into the development of the graphitic structure by calculating the I_D/I_G ratio with increasing HTT, the petroleum coke-derived materials were characterized by Raman spectroscopy. Therefore, a Raman dispersive microscope (Bruker SENTERRA, *Bruker Optics Inc.*) was used operating with a green semiconductor as laser source at a wavelength of 532 nm and 10 mW working power. The samples were focused by a 20× objective. Using an integration time of 60 s, 10 integrations were carried out and conducted. The shown data for the heat-treated samples were taken from our previous publication.[28]

Powder X-ray diffraction measurements (XRD) were performed to investigate the structural changes of the graphitized carbon samples during the heat treatment by calculating the average interlayer spacing (d_{002}), the mean crystallite size along the *c* axis (L_c) and the degree of structural order. The measurements were carried out at a Bruker D8 Advance X-ray powder diffractometer (*Bruker AXS GmbH*) equipped with nickel filtered Cu K_α radiation ($\lambda = 0.154$ nm) in the range of 20° and 35° (2θ) three times per sample. 10 wt% of sieved pure Si powder (Wacker Chemie; grain size: 40–75 μm) was added to the carbon sample for each measurement to avoid possible inaccuracies. Avoiding any influence of absorption only a few mg of material was placed on an oriented Si-wafer sample holder. As described in the work of Iwashita K *et al.* the d_{002}-values were calculated after Lorenz polarization (LP)-correction and peak fitting using Voigt functions.[34] Shown data for graphitized soft carbon was taken from our previous publication.[28]

The carbonized materials were also characterized by nitrogen adsorption measurements using an ASAP 2020 (Accelerated Surface Area and Porosimetry Analyzer, *Micromeritics GmbH*) at 77.3 K (liquid nitrogen temperature). For calculation of the Brunauer-Emmet-Teller (BET) and density functional theory (DFT) surface areas, the standard instrument software and the DFT plus software were used. Data were adopted from our previous studies.[28,32a]

Electrode and cell preparation, and electrochemical characterization

The data of Li^+ ion storage of carbonaceous anodes was taken from our previous study.[28] For electrochemical characterization of K^+ ion storage constant current cycling (CCC) and current rate (C-rate) charge/discharge cycling measurements were performed in lab-scale *Swagelok* type T-cells (three-electrode configuration) using a multichannel Maccor 4300 battery test system at room temperature. As reference and counter electrodes (RE, CE) metallic potassium (99.95% purity, *Sigma-Aldrich*) was used. The working electrode (WE) was prepared as described previously, consisting of 90 wt.% of the carbon active material, 5 wt.% of sodium-carboxymethylcellulose as binder (Na-CMC, Walocel CRT 2000 PPA 12, *Dow Wolff Cellulosics*) and 5 wt.% of the conductive agent Super C65 (*Imerys Graphite & Carbon*).[28] Aluminum foil (*Evonik Industries*, 15 μm thickness) was utilized as current collector for negative electrodes. Active mass loadings were between 2.5 and 3.0 mg cm^{-2}.

1 M potassium bis(fluorosulfonylimide) (KFSI, *Solvionic*; purity: 99.9%) in ethyl methyl carbonate (EMC; *BASF SE*; purity: battery grade) was utilized as electrolyte. A *Whatman* glass microfiber separator (grade GF/D; $Ø = 13$ mm between WE and CE; $Ø = 8$ mm for the RE) was wetted with 120 μL and 80 μL of electrolyte, respectively.

The CCC/C-Rate experiments were performed in the potential range between 0.01 V and 1.5 V vs. $K|K^+$. The theoretical capacity of the anode active material was calculated to be equal to the one of graphite (279 mAh g^{-1}). In the first part, investigating the heat-treated soft carbons, the specific current was set to 279 mA g^{-1} for a rate of 1 C. The first five cycles were performed at 0.1 C (formation cycles) followed by three cycles each at 0.2 C, 0.5 C, 1.0 C and 2.0 C. Afterwards, CCC was continued at 0.5 C to reach 100 cycles in total. These parameters were used to make a fair comparison between potassium related data and previous published lithium related data.[28]

For the investigation of the impact of particle size for commercial graphitic materials, the specific current was set to 279 mA g^{-1} for a rate of 1 C. The first five cycles were performed at 0.1 C (formation cycles), followed by five cycles each at 0.5 C, 1.0 C, 2.0 C and 5.0 C. Afterwards, the cycling was continued at 1.0 C for 500 cycles.

Results and Discussion

Investigation of heat-treated soft carbons

Petroleum coke was heat-treated stepwise at different temperatures in a range between 800 °C and 2800 °C to investigate the impact of the heat treatment temperature (HTT) on the electrochemical performance in PIB cells. In the first part, the obtained carbonaceous materials are characterized regarding the structural characteristics and surface properties. Different techniques like X-ray diffraction (XRD), Raman spectroscopy, nitrogen adsorption measurements, CHN-analysis and scanning electron microscopy were used. In the second part, the obtained samples are electrochemically characterized, and the data is correlated to certain material properties. The shown data of the material characterization has been published previously, however, for evaluation of the Li^+ ion storage behavior.[28]

Material characterization

After HTT, the obtained samples were first characterized via Raman spectroscopy and XRD to investigate the microstructure of the carbonaceous materials. Raman spectroscopy is a useful tool for carbon-based materials which allows to study the presence of graphitic and disordered domains.[35] Figure S1 displays the Raman spectra of all heat-treated samples. In the temperature range of 800 °C to 1600 °C, two broad bands at ≈1350 cm^{-1} and ≈1590 cm^{-1} are mainly present, which can be attributed to disordered-induced (D-band, 1350 cm^{-1}) and ideal graphitic vibration modes (G-band, 1580 cm^{-1}), respectively.[35b,36] With regard to literature, an additional D2-band (1620 cm^{-1}, disorder) and a D3-band (1500 cm^{-1}, disorder) in soft carbons contribute to the peak observed at ≈1590 cm^{-1} which leads to the broadening of the signal, however, plays a minor role for the intensity of the peak.[37] With increasing temperatures (≥1800 °C) a strong growth of two narrow bands at 1580 cm^{-1} and 2695 cm^{-1}, representing the G- and G'-band,[35b,36] can be observed, whereas the D-band decreases. This behavior shows the increase of ordered graphitic domains and a loss of defects and boundaries with increasing temperature. The intensity ratio of D- and G-bands (I_D/I_G) is often used as a well-known indicator to quantify the progress of graphiti-

zation. Figure 1a shows the I_D/I_G ratio in dependence of the HTT. In the range from 800 to 1600 °C, the ratio remains nearly constant at a value of ≈1.0, representative for a highly disordered structure. At 1800 °C the ratio decreases to 0.51, indicating the starting graphitization process, and ends up at a value of 0.07 after treatment at 2800 °C corresponding to a highly graphitic structure. The most obvious changes at temperatures around 1800 °C are consistent with the pre-graphitization step, described in early studies, where carbon layers and crystallites are de-wrinkling. With increasing temperatures above 2000 °C the crystallite growth continues and results in formation of graphitic structures.[38] As a result, the samples from 800 °C to 1800 °C are categorized in the following as "non-graphitized" (marked in Figure 1a as section "I") and above 1800 °C as "graphitized" samples (marked as section "II"). For a further study of the graphitized samples (II), the obtained materials were characterized via XRD (Figure S2). The patterns in Figure S2 show a broad reflection at ≈26 °C 2θ. With increasing temperature, the reflection narrows and shifts to higher 2θ values corresponding to the well-known *00 l* reflection of graphitic carbons at 26.5° 2θ indicating a homogenous graphitization. Based on the *Bragg* equation, the average interlayer distance (d_{002}) was calculated by using the position of the *00 l* reflection and is shown in Figure 1b for temperatures ≥1800 °C. The interlayer spacing decreases from 0.3426 nm (1800 °C) to 0.3359 nm (2800 °C) indicating a convergence to a perfectly stacked graphite with an interlayer spacing of 0.3354 nm. All values are summarized in Tables S1 and S2.

The homogenous graphitization allows to calculate the degree of graphitization (DoG) with respect to the interlayer distance (d_{002}) by using Equation (1):

$$\mathrm{DoG}\ (\%) = \frac{0.3440\ \mathrm{nm} - d_{002}}{0.3440\ \mathrm{nm} - 0.3354\ \mathrm{nm}} \times 100 \quad (1)$$

The value of 0.3440 nm is typical for the interlayer distance of turbostratic carbon and representative for the DoG border of non-graphitizable and graphitizable carbon.[39] The calculated DoGs for the carbon samples are shown in Figure 1b (right axis). Linked to the decreasing interlayer distance, the DoG increases strongly from ≈22% (1800 °C) to ≈93% (2800 °C). Compared to commercial graphite particles, like KS44 (DoG: 99.6%, see Table S3), the DoG at 2800 °C is still very low and disordered domains seem to be still present in the sample. For a higher DoG, treatments at even higher temperatures (> 2800 °C) or longer holding times (>10 h) would be required during graphitization process.

In addition to the microstructure, also the surface characteristics were investigated via nitrogen sorption measurements.

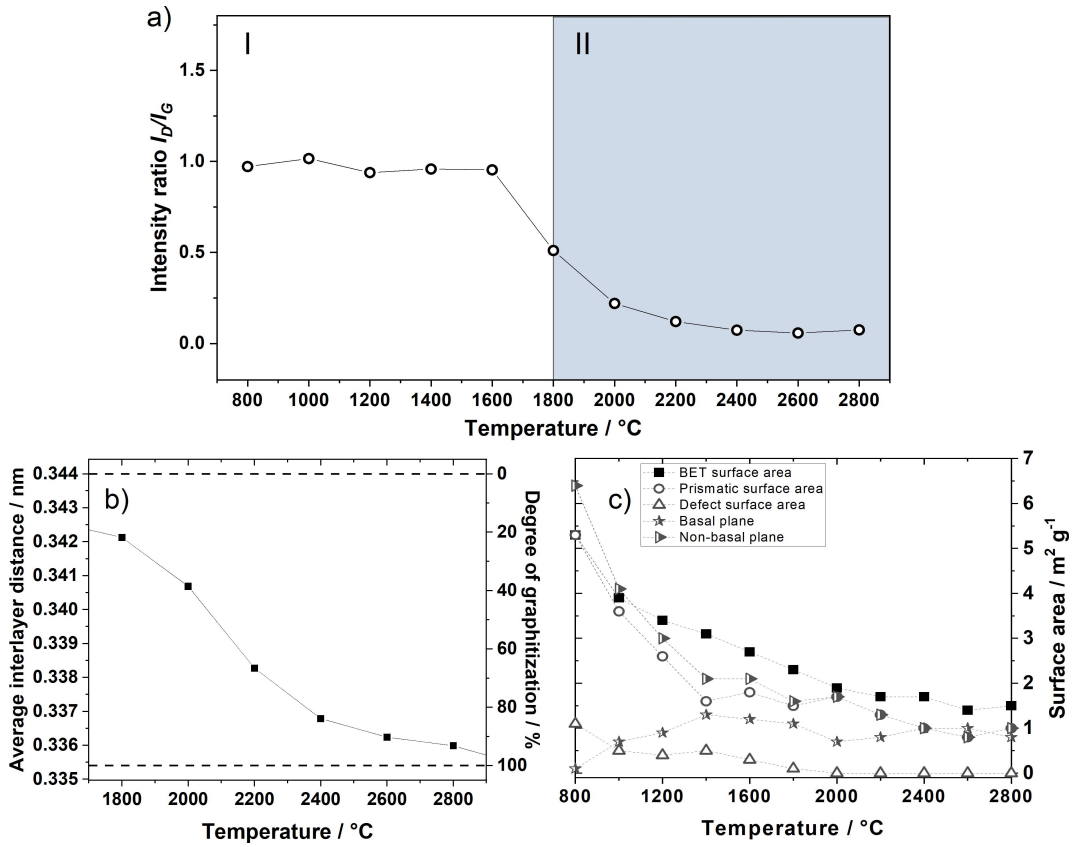

Figure 1. Overview of carbon material characteristics at different HTT: a) I_D/I_G intensity ratios obtained from Raman spectroscopy (compare Figure S1), b) average interlayer distance and degree of graphitization of graphitized (1800–2800 °C) samples obtained from XRD (compare Figure S2), c) BET surface areas and calculated prismatic, defect, basal and non-basal surface areas obtained from nitrogen sorption measurements.

Research Article
doi.org/10.1002/batt.202200045
Chemistry Europe
European Chemical Societies Publishing

The results of the surface analysis are shown in Figure 1c. For all samples, the BET surface area is remarkably low in comparison to commercial graphites (Table S3), which is, however, correlated to the relatively large particle size (D90: 72 ± 3 µm). At 800 °C, a surface area of only 5.3 m^2 g^{-1} was determined. With increasing temperature, the BET surface area decreases strongly ending up with a value of 1.8 $m^2 g^{-1}$. Besides BET surface area, basal-plane and non-basal plane areas of graphitic carbons are known to play an important role for electrochemical performance, e.g., in LIBs.[32a] The amount and ratio of these two different surface types can be calculated via DFT theory[40] and are displayed in Figure 1c. Similar to the BET surface area, also the non-basal plane area decreases strongly with increasing temperature, whereas the absolute basal plane area increases at lower temperatures (up to 1400 °C) and remains nearly constant at > 1600 °C. The non-basal plane can be further divided into prismatic and defect surface area. Figure 1c shows that a defect surface area of 1 $m^2 g^{-1}$ at 800 °C can be measured, which decreases with increasing temperature, whereas no defect surface area is detectable anymore at > 1800 °C.

Electrochemical characterization

The carbon samples obtained from heat treatment were used as electrode material and investigated in carbon | | K metal cells (half-cell setup, three electrode configuration)[41] by constant current charge/discharge cycling experiments. The electrolyte plays also a significant role when materials and their electrochemical performance are analyzed.[42] Therefore, 1 M KFSI in EMC was used as electrolyte, with regard to the literature known stabilized performance of KFSI-based electrolytes in K metal cells.[11,19b,43] For a comparison to lithium-based chemistry as state-of-the-art technology, data from our previous study were used.[28] Figure 2 shows the discharge (= depotassiation/de-lithiation) capacity of the fifth cycle at 0.1 C in dependence of the HTT. In terms of potassium, the obtained disordered soft carbon treated at 800 °C shows a high capacity of 243 mAh g^{-1}. With higher temperatures, the capacity first drops mostly linear to 106 mAh g^{-1} at 1800 °C and increases again to 153 mAh g^{-1} at 2000 °C. In the range from 2000 °C and 2600 °C, the capacity stagnates and even decreases slightly, whereupon at 2800 °C it increases again to 201 mAh g^{-1}. In comparison to Li^+ storage, the course of the discharge capacity

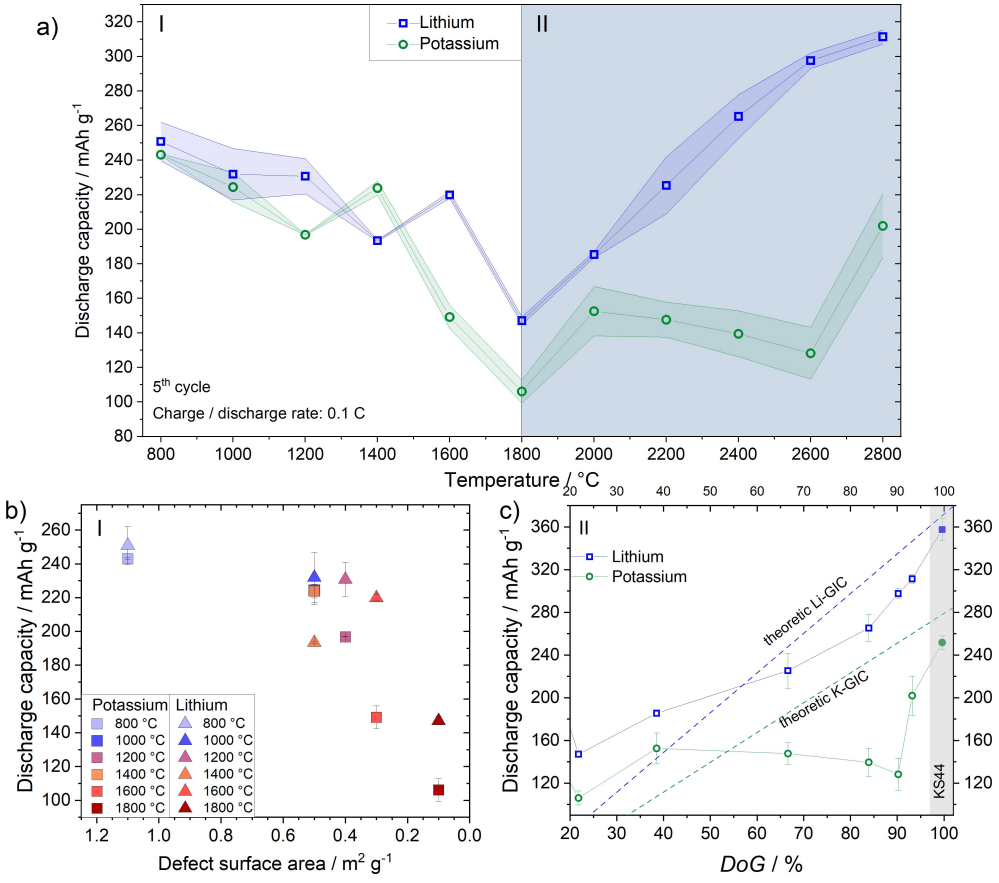

Figure 2. Electrochemical performance of heat-treated carbonaceous materials in carbon | | K metal cells (half-cell setup, three-electrode configuration; CE and RE: K metal, WE: carbons, electrolyte: 1 M KFSI in EMC) compared to performance in carbon | | Li metal cells (half-cell setup, three-electrode configuration; electrolyte: 1 M $LiPF_6$ in EC:DMC 1:1 by vol.). a) Discharge [(de-)potassiation; (de-)lithiation] capacity in the 5th cycle at 0.1 C (1 C = 279 mA g^{-1} for (de-)potassiation or 1 C = 372 mA g^{-1} for (de-)lithiation); b) correlation of discharge capacity and defect surface area. c) Correlation of discharge capacity and degree of graphitization (including data for KS44 graphite). Potential range: 0.01–1.5 V vs. K|K^+. Data for carbon | | Li metal cells were taken from previous publication.[28]

in the low temperature range (800–1400 °C) is very similar. It is worth to mention, that the capacity values for Li^+ and K^+ ion storage are nearly the same. However, with higher temperatures ($\geq$1800 °C) the gap between lithium and potassium increases, and the capacity for Li^+ storage grows strongly without any stagnation to $>$300 mAh g^{-1}.

As described in the previous chapter, the samples can be divided in two sections based on material properties: disordered (I) and ordered carbons (II). This subdivision is also roughly visible in the course of the discharge capacities. In section (I) the capacity decreases with higher temperature, whereas in section (II) the capacity increases with increasing temperature, except for the described stagnation for K^+ ion storage.

To find explanations for this behavior, the development of capacities is considered from different perspectives. Previous studies showed that for disordered soft carbons a surface-driven adsorption mechanism is mainly dominant, whereas for ordered graphitic carbons an intercalation mechanism can be observed, which was proven by in situ Raman and XRD studies[30a] as well as cyclic voltammetry experiments.[31] However, to the best of our knowledge, no systematic analysis of special surface properties obtained *via* gas adsorption measurement has been performed yet combined with correlated electrochemical performance of soft carbons. For further and deeper understanding of the stated surface-driven mechanism, the obtained discharge capacities for the samples in section (I) were analyzed with respect to measured surface properties. Figure S3 displays the correlation of specific discharge capacity and BET surface area for K^+ and Li^+ storage. For both chemistries, a rough trend can be observed. With decreasing BET surface area, the discharge capacity decreases. However, in the range of 4.0–3.0 m^2 g^{-1} the correlation is not very clear. A further important property for the ion adsorption storage mechanism is the number of defects.[44] Figure 2b shows the discharge capacity of the 5th cycle in dependence of the defect surface area for samples treated at temperatures between 800 °C and 1800 °C. It is clearly visible that the discharge capacity decreases also with a lower defect surface area, but the correlation seems not to be linear. For K^+ storage (squares), the discharge capacity decreases only slowly between 1.1 m^2 g^{-1} and 0.5 m^2 g^{-1} (243 mAh g^{-1} to 224 mAh g^{-1}), whereas below 0.5 m^2 g^{-1}, the capacity drops strongly with decreasing defect surface area to 106 mAh g^{-1} at 0.1 m^2 g^{-1}. It is noticeable that the samples treated at 1000 °C and 1400 °C achieve similar capacities and possess the same defect surface area, which could explain the outlier for 1400 °C observed in Figure 2a, and strengthen the correlation of defect surface area and capacity for disordered carbons.

Moreover, this observed trend is similar for Li^+ ion storage, although the capacity drops not as strongly as for K^+ ion storage where the defect surface area falls below 0.5 m^2 g^{-1}. Besides defects, also the prismatic surface area, which is plotted in Figure S3, is well-known to play a role for adsorption mechanism confirming the described trends.[32a] The strong correlation of BET, prismatic and especially defect surface areas with the discharge capacity for disordered soft carbons supports the hypothesis of a surface-driven adsorption mechanism. Therefore, the defect surface area might be considered as an indicator for the disordered bulk structure of the carbon material, which enables the adsorption storage mechanism. These results give further insights into the storage mechanism and show the importance of surface-controlled and -optimized soft carbons. For further validation of the intercalation/insertion *vs.* adsorption processes, it might be helpful to analyze core-shell type carbon materials, i.e., graphite core/amorphous shell materials *vs.* amorphous core/graphite shell materials.

In section (II) of the chosen HTT window, the obtained carbonaceous materials start to develop an ordered graphitic structure. By correlating the achieved discharge capacities of section (II) with surface properties (see Figure S4), no clear trends can be observed. In contrary, the discharge capacity even increases with lower BET surface area. This observation supports the hypothesis, that surface-driven adsorption K storage mechanism can be neglected at temperatures $>$1800 °C and is replaced by an intercalation K storage mechanism. To investigate the dependence of the capacity from graphitization progress, the discharge capacity for Li^+ and K^+ ion storage is plotted against the calculated DoG in Figure 2c. In addition to the highest temperature, the capacity of commercial graphite KS44 was added in Figure 2c to compare with a graphitic carbon with similar particle morphology (see Figure S5) but higher DoG, since the DoG of the sample obtained at 2800 °C is only limited to 93 %. The course of capacity in dependence of DoG looks similar to Figure 2a for both, Li^+ and K^+ storage, which is caused by the nearly linear increase of the DoG with higher temperatures (see Figure 1b). The theoretical capacities of a Li- and K-based GICs (372 mAh g^{-1} for LiC_6 and 279 mAh g^{-1} for KC_8) are multiplied with the degree of graphitization and are displayed as dotted lines to estimate the contribution of the intercalation mechanism for ordered carbons (Figure 2c). These lines allow to estimate the contribution of the developed graphitic domains to the overall capacity. At lower DoG and with that, at lower HTT, the achieved capacity exceeds the theoretical achievable values by formation of a GIC for both chemistries. This means that not only intercalation, but also surface-driven adsorption mechanisms seem to still contribute to the capacity. At a DoG of $>$50 % the theoretical capacity of the GIC exceeds the achieved capacity for both chemistries. However, for K^+ storage the capacity stagnates with increasing DoG until a value of 90 % is reached. At this point, the capacity increases steeply again and reaches nearly the theoretical possible capacity by forming KC_8. Based on these results, it can be assumed that for K^+ storage a high DoG is even more mandatory than for Li^+ storage to achieve high capacities close to the theoretical value. This observation is in line with previous studies about the influence of crystallinity for synthetic graphite. Igarashi et al. showed that the crystallinity of graphite is a predominant factor for K^+ intercalation and application as negative electrode material.[45]

A further important performance indicator for the practical application of electrode active materials is the Coulombic efficiency (C_{Eff}). For Li^+ ion storage the impact of surface area as

well as of non-basal planes including defect and prismatic surface areas were shown in early studies.[32a] It is well-known, that a high surface area as well as a high amount of non-basal planes lead to lower initial C_{Eff}.[32b] To confirm such a behavior for K^+ ion storage, the C_{Eff} of the first cycle was investigated with regard to different surface properties.

Figure 3a shows the C_{Eff} in dependence of the HTT. For carbon || Li metal cells, the C_{Eff} increases with higher temperature, apart from the obtained sample at 2000 °C. In terms of carbon || K metal cells, the C_{Eff} decreases from 800 °C to 1600 °C, except of the obtained sample at 1400 °C and increases again at temperatures >1600 °C. To shed more light on this unexpected behavior, Figure 3b displays the C_{Eff} against the BET surface area for all heat-treated samples (section I+II). For Li^+ storage, the C_{Eff} increases clearly with decreasing surface area as expected, even though the obtained sample at 2000 °C differs strongly. For K^+ storage, the trend is not clear due to the high C_{Eff} at high BET surface area and two lower C_{Eff} values at moderate surface areas. However, splitting up the charts into ordered (section I) and disordered (section II) carbons, the described expected trend can be observed for the ordered carbons in section II, where the BET surface area clearly correlates with the C_{Eff} (Figure S6). For the disordered carbons in section I, no clear trend is visible. This phenomenon is also observed for the non-basal surface area including defects and primary planes. For section II the C_{Eff} increases with a lower number of non-basal plane area, whereas for section I no clear trend could be identified for any surface area (Figure S6). Based on these results, it seems to be the case that the well-known correlation of surface area and C_{Eff} is not clear for K^+ storage in disordered carbons. Only for ordered carbonaceous materials, known trends from Li^+ storage can be transferred to the K-based chemistry following similar rules.

Figure 4a and b shows potential profiles for potassiation (a) and de-potassation (b) of carbon || K metal cells for selected materials obtained at different HTT. It is visible that the (de-)potassiation is shifted to lower values with increasing HTT caused by the development of an ordered graphitic structure. For disordered carbon obtained at 800 °C, potassiation already starts at 1.0 V vs. $K|K^+$ followed by a typical sloping potential behavior. At temperatures >2200 °C, potassiation starts at ≈0.3 V vs. $K|K^+$ showing a clear plateau caused by the staging intercalation mechanism.[46] In Figure 4c and b the cyclic potential profiles of Li^+ and K^+ storage of carbons obtained at 800 °C and 2800 °C are displayed. In terms of disordered carbons, a similar sloping behavior is visible for both chemistries with a low voltage hysteresis. For the carbons obtained at 2800 °C, a strong difference between Li^+ and K^+

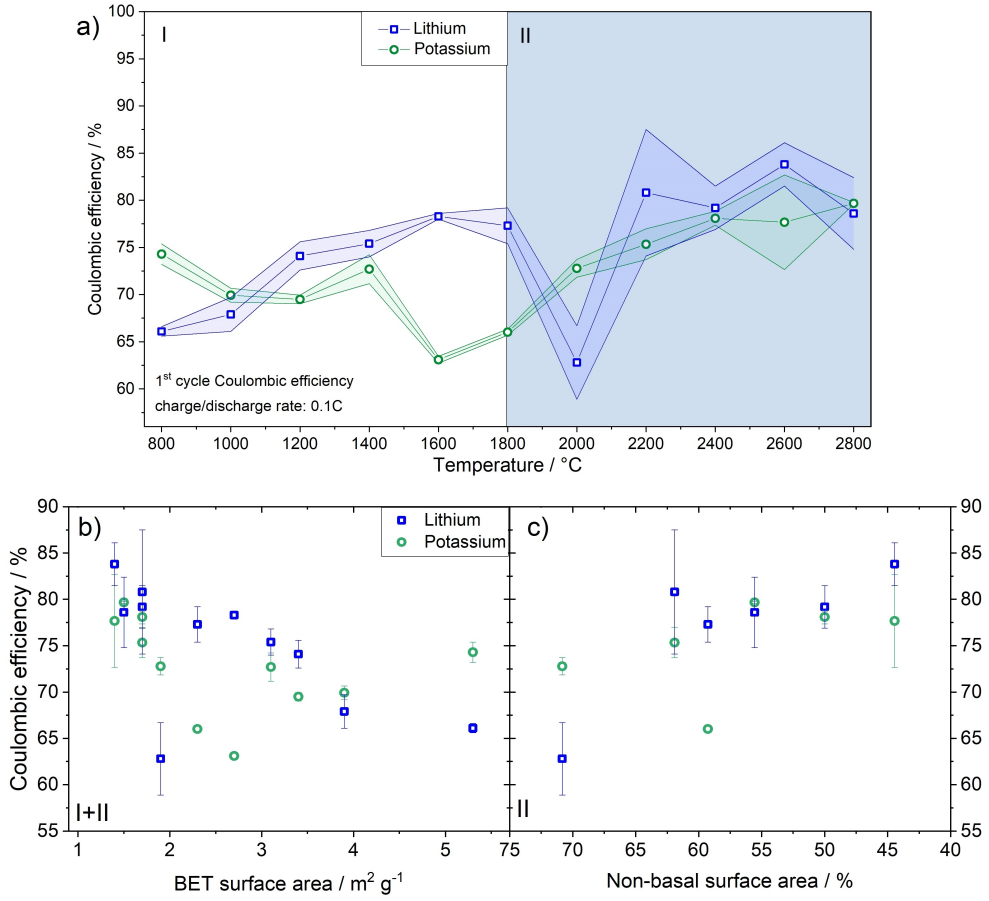

Figure 3. Development of first cycle Coulombic efficiency of carbon || K metal cells in dependence of a) HTT, b) BET surface area (800–2800 °C) and c) non-basal surface area (1800–2800 °C). Data for carbon || Li metal cells were taken from previous publication.[28]

Research Article
doi.org/10.1002/batt.202200045
Chemistry Europe
European Chemical Societies Publishing

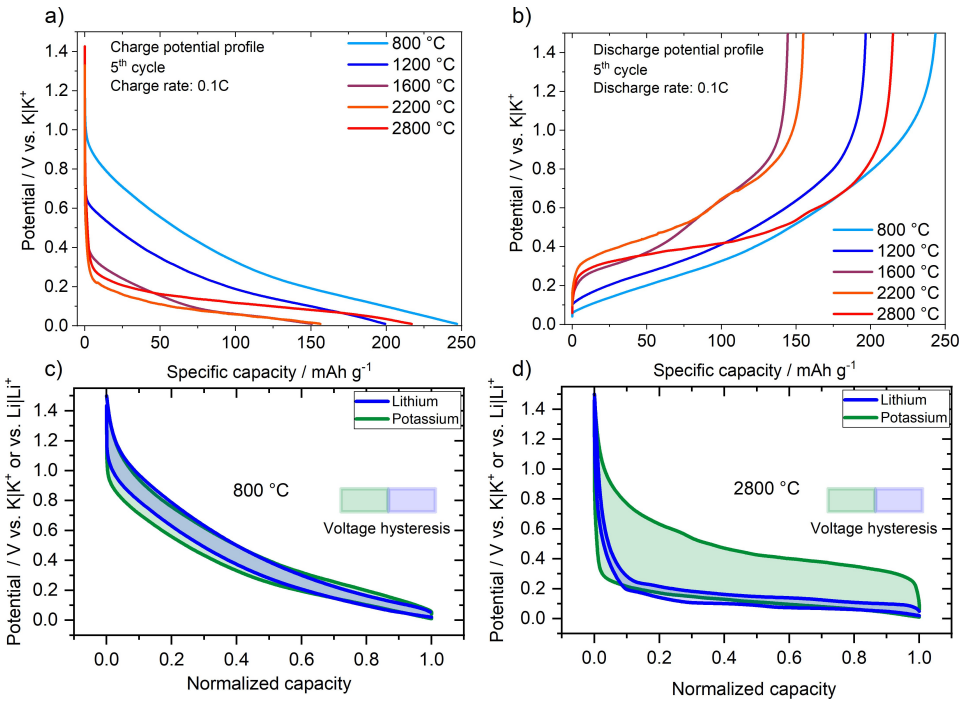

Figure 4. a) Charge (potassiation) and b) discharge (de-potassiation) potential profiles of the 5th cycle for carbons obtained at different temperatures cycled in carbon | | K metal cells (half-cell setup, three-electrode configuration; CE and RE: K metal, WE: carbonaceous materials, electrolyte: 1 M KFSI in EMC). c and d): Cyclic potential profiles of the 5th cycle for Li^+ and K^+ ion storage against normalized capacity for carbons obtained at c) 800 °C and d) 2800 °C. Potential range: 0.01–1.5 V vs. $K|K^+$. Data for carbon | | Li metal cells were taken from previous publication.[28]

ion storage is visible. The potassium potential profile exhibits a strong voltage hysteresis (> 0.3 V) compared to Li^+ storage (< 0.1 V) which is also described in earlier studies.[11]

In further cycling experiments, the rate capability and cycling stability of all obtained materials were investigated in carbon | |K metal cells (Figure S7). Representative performance data for disordered carbon (800 °C) and ordered carbon (2800 °C) are discussed in more detail. Figure S8 displays the de-potassiation capacities at different C-rates. The disordered soft carbon clearly outperforms the graphitic ordered carbon in terms of specific capacity at different rates. The ordered carbon only achieves ≈50 % of the capacity at 0.5 C compared to the value at 0.1 C, whereas the disordered one still achieves ≈80 %. This behavior shows a very poor rate capability for samples with increased graphitic ordering. The sluggish kinetics of K^+ ion intercalation into graphite is often referred as one disadvantage of graphitic carbons as negative electrode material compared to soft carbons and is explained by the limited diffusion.[30] This claimed disadvantage of graphite is often used to question a potential application of graphite in possible future PIB cells. However, important characteristics of graphitic anodes are also the particle size and morphology, which has been rarely addressed systematically in literature so far.[46b] In general, the particle size as well as the particle morphology have a strong impact on the electrochemical performance. Especially for graphite negative electrodes in LIB cells strong effects on the rate capability and C_{Eff} in the first charge/discharge cycle can be observed,[47] whereas the characteristics of graphite as a positive electrode in a dual-ion cells play a minor role.[48] In this study, the D90 particle size distribution of the carbon obtained at 2800 °C was determined to be ≈72 μm, which is significantly larger than that of commercial graphites used in LIB cells (< 30 μm). Therefore, commercial graphites with high degree of graphitization and different particle sizes were investigated with regard to their electrochemical performance to understand the impact of the particle size on cell performance.

Impact of particle size on electrochemical performance

Different commercial graphites with a flake-like morphology were selected to gain insights into the impact of particle size on K^+ ion storage (Table S3).

The choice of the different graphite materials was made regarding different D90 particle size distributions to cover a broad range of different particle sizes and surface areas. The materials were investigated by charge/discharge experiments at different rates of 0.1 C, 0.5 C, 1 C, 2 C and 5 C (1 C = 279 mA g^{-1}). Figure 5a displays the specific capacity of the third cycle for all graphitic carbons at different C-rates. For all graphite materials, a decay of capacity with higher C-rate can be observed (compare Figure S9). KS4 shows an exceptionally small loss of capacity, whereas SFG44 undergoes a strong capacity decay for C-rates higher than 0.5 C. This behavior can be correlated to the increased particle size. Figure 5b shows the capacity retention at different C-rates in dependence of the particle size distribution (D90). To ensure a fair comparison

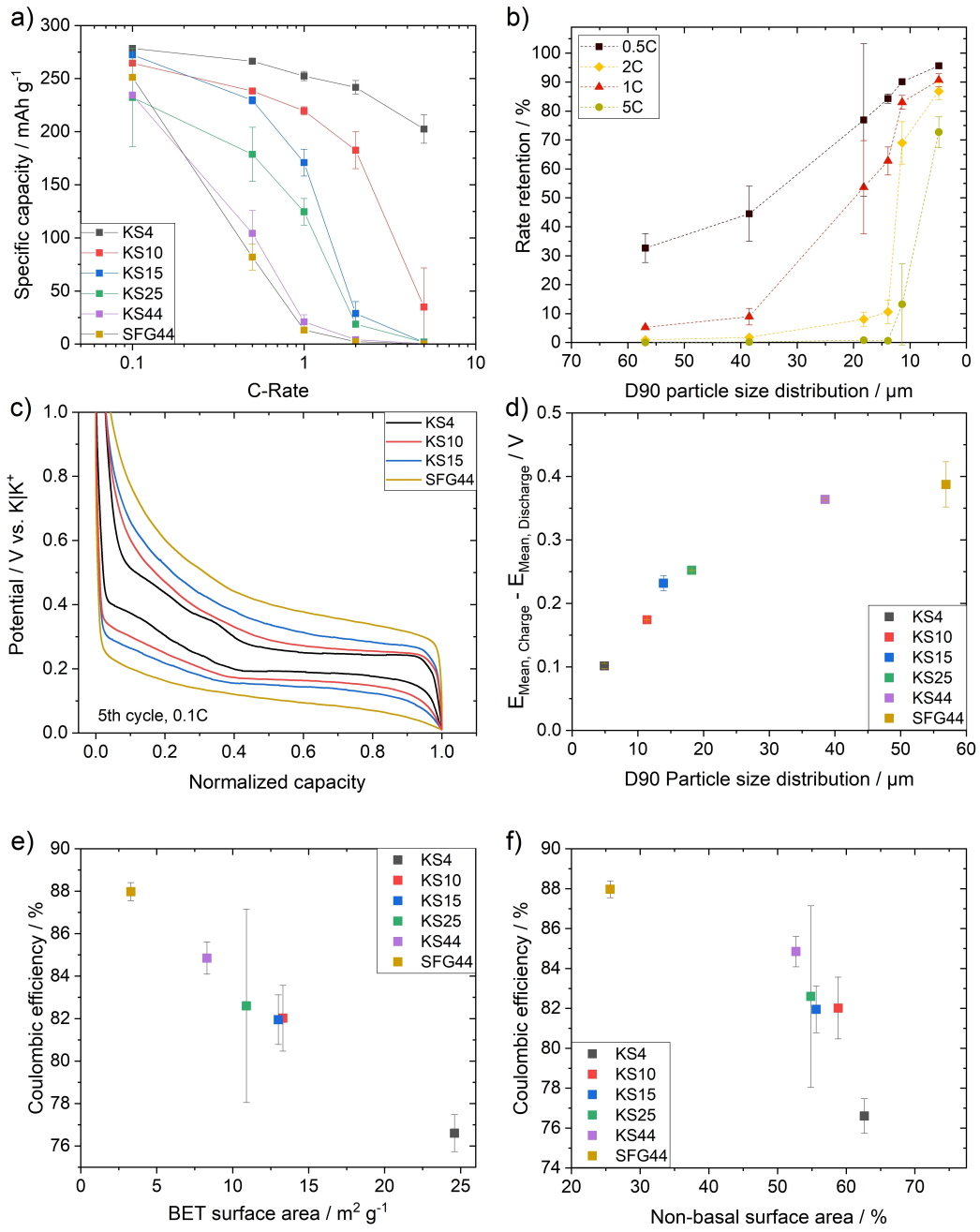

Figure 5. Electrochemical performance of different commercial graphites in graphite||K metal cells (half-cell setup; three-electrode cells, CE and RE: K metal, WE: graphites, electrolyte: 1 M KFSI in EMC). Potential range: 0.01–1.5 V vs. K|K$^+$. a) Specific discharge (de-potassiation) capacity in the 3rd cycle at different current rates, b) rate retention in dependence of the D90 particle size distribution, c) potential profiles of the 5th cycle at 0.1 C, d) voltage hysteresis of the 5th cycle at 0.1 C in dependence of D90 value, e and f) first cycle Coulombic efficiency in dependence of e) BET surface area and f) portion of "non-basal" surface area.

considering the slightly different capacities at 0.1 C, a "rate retention" was calculated, which is described as percentage of achieved capacity at a given C-rate in relation to the capacity at 0.1 C. The rate retention at all C-rates decreases strongly with increasing D90 value. For the lowest particle size distribution (D90: 4.9 µm, KS4) 86% of capacity is still achievable at 2 C and even 73% at 5 C. This behavior demonstrates the power of particle design and influence of the particle size on the claimed poor rate capability. It can be stated that the claimed slow diffusion of K^+ ion inside of graphite even strengthens the effect of the particle size and underlines the importance of particle design for possible future applications.

Furthermore, the different graphitic materials also show a huge difference in their potential profile. Figure 5c displays the potential profiles of the 5th cycle at 0.1 C for representative carbon || K metal cells. KS4 shows a typical profile during potassiation, dominated by a staging behavior with an on-set potential of ≈0.4 V vs. K|K$^+$. With increasing particle size, the

staging plateaus more and more diminish, and the on-set potential is lowered to a value of 0.25 V vs. $K|K^+$ for SFG44. A similar trend can be seen for the de-potassiation profiles. A clear staging behavior is visible for KS4, whereas the de-potassiation profile is shifted to higher values for SFG44, and the plateaus seem to be smeared. It can be stated that the enhanced voltage hysteresis, which is often mentioned as disadvantage for possible application, is influenced by the particle design. To find out more about possible correlations with material properties, Figure 5c shows the voltage hysteresis of different graphites, defined as difference between mean charge (potassiation) and mean discharge (de-potassiation) potential, in dependence of the D90 particle size distribution. Based on this correlation, it can be assumed that the voltage hysteresis increases significantly with larger particle sizes. This effect could be explained by the claimed low diffusion kinetics of K^+ ions inside of graphitic domains.[30] With increasing particle size, the length of diffusion paths inside graphitic particles are increased and with that overpotentials are generated. However, it should be kept in mind, that with lower particle size also the specific surface area increases (Table S3). With that, also the effective current density differs since the same specific, mass-related, current was applied. In comparison, KS4 possesses a 7.5 times higher surface area than SFG44 (Table S3) and therefore experiences theoretically a maximum 7.5 times lower current density considering only the surface area of the pure graphitic powder. However, by manufacturing the composite electrode, the electrochemically active surface area should be decreased slightly and with that also the difference between KS4 and SFG44. Nevertheless, to estimate the effect of a possible lower effective current density on the voltage hysteresis due to the higher surface area of KS4, potential profiles of KS4 at five and ten times higher specific current rates (0.5 C and 1 C) are compared to the potential profile of SFG44 at 0.1 C in Figure S10. It can be observed, that with higher current rates, the potassiation plateaus are shifted to lower potentials, whereas the de-potassiation potentials increase. As a result, the voltage hysteresis increases with higher current rates. However, even at ten times higher specific current KS4 exhibits still a lower hysteresis and a more pronounced staging profile than SFG44. This observation suggests that the effect of a stronger hysteresis is related to a higher current density due to the lower surface area but is even more affected by larger particle sizes and longer diffusion paths.

On the other hand, also the different surface properties could play an important role determining kinetics of K^+ ion uptake. In Figure S11, the voltage hysteresis is plotted against the BET surface area, absolute "non-basal plane" surface area and the percentage of non-basal planes. Considering the intercalation mechanism of large K^+ ions via the prismatic plane, especially the proportion of non-basal planes should be a determining factor for limiting kinetics and possible overpotentials, which effects the voltage hysteresis. For a proportion of more than 55% of non-basal planes, the voltage hysteresis strongly decreases with an increasing portion of non-basal planes. To summarize theses correlations, both parameters, particle size and surface properties, especially the portion of non-basal planes, play an important role for the overall kinetics of graphite-based electrodes in PIB cells including rate capability and voltage hysteresis.

Graphites with similar particle size distribution but different non-basal plane ratios should be investigated in future studies to quantify and clearly separate the influence of both parameters. A further performance indicator, which is affected by the particle design, is the C_{Eff}. Figure 5e and f shows the first cycle C_{Eff} in dependence of the BET surface area and basal surface area ratio. In the first part of this study, it was already observed that the C_{Eff} decreases with higher surface area for graphitic ordered carbons. This trend is confirmed by analysis of commercial graphites. SFG44 with the lowest BET surface area (3.3 $m^2 g^{-1}$) shows a high initial C_{Eff} of 87.9%, whereas KS4 suffers from a low initial C_{Eff} of 76.6%. Considering the intercalation mechanism of K^+ into graphite via the prismatic plane and the related solid electrolyte interphase (SEI) formation, the initial C_{Eff} often correlates significantly with the non-basal-planes, as known for LIB cells.[32] Figure 5f displays the initial C_{Eff} in dependence of the ratio of non-basal surface area. Also, the C_{Eff} decreases with increasing non-basal surface area, which can be explained by a possible enhanced electrolyte decomposition and SEI formation on prismatic planes. Both correlations support the results demonstrated in the first part of the study.

Overall, the results show that the particle design strongly influences the performance of graphite for K^+ ion intercalation. Small particle sizes are very important to achieve a promising rate capability, small voltage hysteresis (thus high voltage efficiency[49]) and to buffer also the volumetric expansion during K^+ intercalation. Keeping this in mind, KS4 shows a promising performance with outstanding rate capability and high cycle stability. Figure 6 shows the long-term cycling performance of KS4 graphite||K metal cells at 1 C. After 500 cycles a capacity of 181 mAh g^{-1} is still achieved demonstrating a high-capacity retention of 72% (500^{th} to 30^{th} cycle). Furthermore, a high C_{Eff} of $>99.9\%$ is reached showing the practicability of graphitic anodes for PIBs.

Conclusion

In this work, a comprehensive study about the impact of different particle, structure and surface parameters for disordered soft carbons and ordered graphitic carbons on the electrochemical performance for K^+ ion storage is presented. First, petroleum coke as industrial precursor for artificial graphite and soft carbons, was heat-treated from 800 °C to 2800 °C in 200 °C steps and analyzed regarding the degree of graphitization *via* Raman spectroscopy and XRD as well as to surface properties via nitrogen adsorption measurements. Based on the material characterization, the obtained materials were divided into two sections: disordered (800 °C–1800 °C) and ordered graphitic carbons (1800 °C–2800 °C). Constant current charge/discharge experiments in carbon || K metal cells were performed to correlate electrochemical performance indicators

Research Article
doi.org/10.1002/batt.202200045
Chemistry Europe
European Chemical Societies Publishing

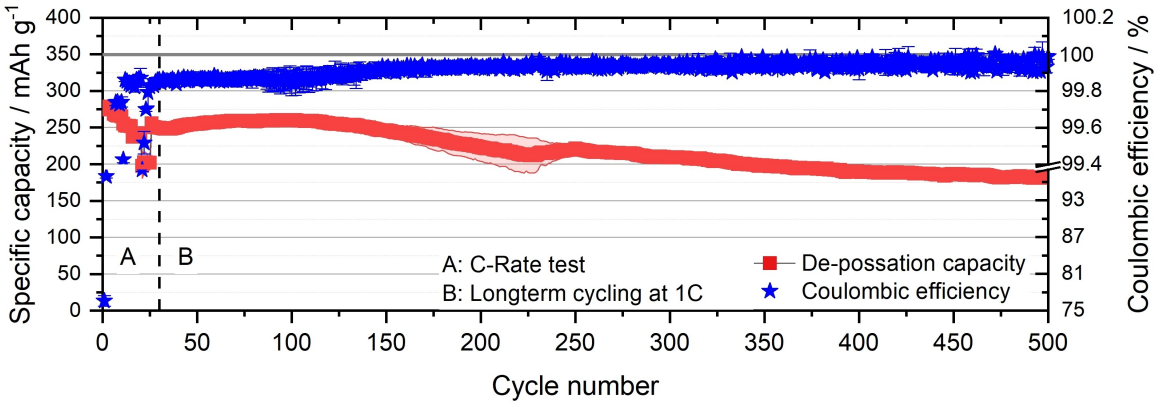

Figure 6. Specific discharge (de-potassiation) capacity and Coulombic efficiency of KS4 graphite||K metal cells (half-cell setup; three-electrode cells, CE and RE: K metal, WE: KS4, electrolyte: 1 M KFSI in EMC; Potential range: 0.01–1.5 V vs. K|K$^+$).

with material properties and compared to results obtained for Li^+ ion storage. For disordered carbons, similar specific capacities for Li^+ and K^+ ion storage were detected. The specific capacity strongly correlates with the defect surface area of the disordered carbons confirming the surface-driven adsorption mechanism of K^+ and Li^+ ion storage in disordered soft carbons. However, no clear trend could be observed for the correlation of Coulombic efficiency (C_{Eff}) and surface properties for K^+ ion storage in disordered carbons.

The capacity of ordered graphitic carbons was linked to the degree of graphitization (DoG). In comparison to Li^+ ion storage, an increased DoG seems to be mandatory to achieve moderate capacity close to the theoretical value. For ordered graphitic carbons, a clear trend was observed for the C_{Eff} and surface properties. As expected, the C_{Eff} is closely linked with the BET surface area and area non-basal plane area. Comparing the kinetics of highly disordered carbon obtained at 800 °C and graphitic ordered carbon heat-treated at 2800 °C, the disordered carbon clearly outperforms the graphitic material, the latter also suffers from a strong voltage hysteresis.

However, supposed disadvantages of graphitic carbons, like poor rate capability and strong voltage hysteresis, were further investigated in a second part of the study, by analyzing the electrochemical performance of commercial flake-like graphite with different particle size distributions in graphite||K metal cells. It was clearly shown that the rate capability is strongly influenced by the particle size. Utilizing KS4, with a low D90 particle size distribution value of 4.9 µm, a capacity of 202 mAh g^{-1} at 5 C could be achieved, representing a high-capacity retention of 76.6% compared to 0.1 C. Furthermore, the voltage hysteresis could be closely linked to particle size and surface area properties of graphitic carbons. By decreasing the particle size and increasing non-basal planes the voltage hysteresis was strongly reduced. However, the large surface area and high portion of non-basal planes of KS4 was found to cause a low first cycle C_{Eff}.

To summarize, these results show important insights into the correlation of material properties and electrochemical performance for carbonaceous anodes and emphasize the significant impact of particle, structure, and surface design for optimum K^+ ion storage capabilities. The optimization of the particle morphology of graphitic negative electrode materials can overcome known issues of graphitic potassium storage anodes like low kinetics and large voltage hysteresis to pave the path towards future application of PIB cells.

Acknowledgements

We wish to thank the Ministry of Economic Affairs, Innovation, Digitalization and Energy of the State of North Rhine-Westphalia (MWIDE) for funding this work in the project "GrEEn" (313-W044A). The authors also thank Andre Bar for his graphical support. Open Access funding enabled and organized by Projekt DEAL.

Conflict of Interest

The authors declare no conflict of interest.

Data Availability Statement

The data that support the findings of this study are available from the corresponding author upon reasonable request.

Keywords: carbonaceous anodes · degree of graphitization · graphite · potassium-ion batteries · voltage hysteresis

[1] a) R. Schmuch, R. Wagner, G. Hörpel, T. Placke, M. Winter, *Nat. Energy* **2018**, *3*, 267–278; b) M. Winter, B. Barnett, K. Xu, *Chem. Rev.* **2018**, *118*, 11433–11456; c) T. Placke, R. Kloepsch, S. Dühnen, M. Winter, *J. Solid State Electrochem.* **2017**, *21*, 1939–1964; d) G. E. Blomgren, *J. Electrochem. Soc.* **2016**, *164*, A5019.
[2] B. Dunn, H. Kamath, J.-M. Tarascon, *Science* **2011**, *334*, 928–935.
[3] European Commision, *Critical Raw Materials Resilience: Charting a Path towards greater Security and Sustainability*, *COM(2020) 474 final*, **2020**; Accessed: 10.01.2022 [https://eur-lex.europa.eu/legal-content/EN/TXT/?uri=CELEX:52020DC0474].

[4] C. B. Tabelin, J. Dallas, S. Casanova, T. Pelech, G. Bournival, S. Saydam, I. Canbulat, *Miner. Eng.* **2021**, *163*, 106743.
[5] a) P. K. Nayak, L. Yang, W. Brehm, P. Adelhelm, *Angew. Chem. Int. Ed.* **2018**, *57*, 102–120; *Angew. Chem.* **2018**, *130*, 106–126; b) J. C. Pramudita, D. Sehrawat, D. Goonetilleke, N. Sharma, *Adv. Energy Mater.* **2017**, *7*, 1602911.
[6] a) D. Aurbach, Z. Lu, A. Schechter, Y. Gofer, H. Gizbar, R. Turgeman, Y. Cohen, M. Moshkovich, E. Levi, *Nature* **2000**, *407*, 724–727; b) J. O. Besenhard, M. Winter, *ChemPhysChem* **2002**, *3*, 155–159.
[7] J. Park, Z. L. Xu, G. Yoon, S. K. Park, J. Wang, H. Hyun, H. Park, J. Lim, Y. J. Ko, Y. S. Yun, *Adv. Mater.* **2019**, *32*, 1904411.
[8] a) T. Hosaka, K. Kubota, A. S. Hameed, S. Komaba, *Chem. Rev.* **2020**; b) A. Eftekhari, Z. Jian, X. Ji, *ACS Appl. Mater. Interfaces* **2016**, *9*, 4404–4419; c) Z. Zhang, Y. Du, Q. C. Wang, J. Xu, Y. N. Zhou, J. Bao, J. Shen, X. Zhou, *Angew. Chem. Int. Ed.* **2020**, *59*, 17504–17510; *Angew. Chem.* **2020**, *132*, 17657–17663; d) B. Cao, X. Li, *Acta Physico-Chimica Sinica* **2020**, *36*, 89.
[9] a) R. D. Shannon, *Acta Crystallogr. Sect. A* **1976**, *32*, 751–767; b) J. M. Wrogemann, I. A. Rodríguez-Pérez, M. Winter, T. Placke, in *Front. Nanosci., Vol. 19*, Elsevier, **2021**, pp. 273–325.
[10] M. Okoshi, Y. Yamada, S. Komaba, A. Yamada, H. Nakai, *J. Electrochem. Soc.* **2017**, *164*, A54–A60.
[11] S. Komaba, T. Hasegawa, M. Dahbi, K. Kubota, *Electrochem. Commun.* **2015**, *60*, 172–175.
[12] a) J. Dahn, *Phys. Rev. B* **1991**, *44*, 9170; b) T. Ohzuku, Y. Iwakoshi, K. Sawai, *J. Electrochem. Soc.* **1993**, *140*, 2490; c) T. Tran, K. Kinoshita, *J. Electroanal. Chem.* **1995**, *386*, 221–224.
[13] Z. Jian, W. Luo, X. Ji, *J. Am. Chem. Soc.* **2015**, *137*, 11566–11569.
[14] a) D. Stevens, J. Dahn, *J. Electrochem. Soc.* **2001**, *148*, A803-A811; b) P. Ge, M. Fouletier, *Solid State Ionics* **1988**, *28*, 1172–1175.
[15] a) H. Kim, J. Hong, Y. U. Park, J. Kim, I. Hwang, K. Kang, *Adv. Funct. Mater.* **2015**, *25*, 534–541; b) Z. Zhu, F. Cheng, Z. Hu, Z. Niu, J. Chen, *J. Power Sources* **2015**, *293*, 626–634; c) J. Xu, Y. Dou, Z. Wei, J. Ma, Y. Deng, Y. Li, H. Liu, S. Dou, *Adv. Sci.* **2017**, *4*, 1700146; d) Y. Li, Y. Lu, P. Adelhelm, M.-M. Titirici, Y.-S. Hu, *Chem. Soc. Rev.* **2019**, *48*, 4655–4687.
[16] a) R. Rajagopalan, Y. Tang, X. Ji, C. Jia, H. Wang, *Adv. Funct. Mater.* **2020**, 1909486; b) J. Liao, C. Chen, Q. Hu, Y. Du, Y. He, Y. Xu, Z. Zhang, X. Zhou, *Angew. Chem. Int. Ed.* **2021**, *60*, 25575–25582.
[17] a) X. Wang, K. Han, D. Qin, Q. Li, C. Wang, C. Niu, L. Mai, *Nanoscale* **2017**, *9*, 18216–18222; b) Y. Liu, Y. X. Lu, Y. S. Xu, Q. S. Meng, J. C. Gao, Y. G. Sun, Y. S. Hu, B. B. Chang, C. T. Liu, A. M. Cao, *Adv. Mater.* **2020**, *32*, 2000505.
[18] a) Z. Jian, Z. Xing, C. Bommier, Z. Li, X. Ji, *Adv. Energy Mater.* **2016**, *6*, 1501874; b) Z. Jian, S. Hwang, Z. Li, A. S. Hernandez, X. Wang, Z. Xing, D. Su, X. Ji, *Adv. Funct. Mater.* **2017**, *27*, 1700324; c) Z. Xu, S. Du, Z. Yi, J. Han, C. Lai, Y. Xu, X. Zhou, *ACS Appl. Energ. Mater.* **2020**, *3*, 11410–11417.
[19] a) H. Kim, G. Yoon, K. Lim, K. Kang, *Chem. Commun.* **2016**, *52*, 12618–12621; b) L. Fan, R. Ma, Q. Zhang, X. Jia, B. Lu, *Angew. Chem. Int. Ed.* **2019**, *58*, 10500–10505; *Angew. Chem.* **2019**, *131*, 10610–10615.
[20] B. Cao, Q. Zhang, H. Liu, B. Xu, S. Zhang, T. Zhou, J. Mao, W. K. Pang, Z. Guo, A. Li, J. Zhou, X. Chen, H. Song, *Adv. Energy Mater.* **2018**, *8*, 1801149.
[21] Q. Liu, F. Han, J. Zhou, Y. Li, L. Chen, F. Zhang, D. Zhou, C. Ye, J. Yang, X. Wu, *ACS Appl. Mater. Interfaces* **2020**, *12*, 20838–20848.
[22] I. Sultana, M. M. Rahman, T. Ramireddy, Y. Chen, A. M. Glushenkov, *J. Mater. Chem. A* **2017**, *5*, 23506–23512.
[23] a) J. Zheng, Y. Yang, X. Fan, G. Ji, X. Ji, H. Wang, S. Hou, M. R. Zachariah, C. Wang, *Energy Environ. Sci.* **2019**, *12*, 615–623; b) J. Wang, Z. Liu, J. Zhou, K. Han, B. Lu, *ACS Materials Lett.* **2021**, *3*, 1572–1598.
[24] B. Tian, W. Tang, K. Leng, Z. Chen, S. J. R. Tan, C. Peng, G.-H. Ning, W. Fu, C. Su, G. W. Zheng, *ACS Energy Lett.* **2017**, *2*, 1835–1840.
[25] I. Sultana, M. M. Rahman, S. Mateti, V. G. Ahmadabadi, A. M. Glushenkov, Y. Chen, *Nanoscale* **2017**, *9*, 3646–3654.
[26] a) J. Yang, Y. Zhai, X. Zhang, E. Zhang, H. Wang, X. Liu, F. Xu, S. Kaskel, *Adv. Energy Mater.* **2021**, *11*, 2100856; b) J. Yang, Z. Ju, Y. Jiang, Z. Xing, B. Xi, J. Feng, S. Xiong, *Adv. Mater.* **2018**, *30*, 1700104.
[27] S. Tian, Y. Zhang, C. Yang, S. Tie, J. Nan, *Electrochim. Acta* **2021**, *380*, 138254.
[28] O. Fromm, A. Heckmann, U. C. Rodehorst, J. Frerichs, D. Becker, M. Winter, T. Placke, *Carbon* **2018**, *128*, 147–163.
[29] A. Heckmann, O. Fromm, U. Rodehorst, P. Münster, M. Winter, T. Placke, *Carbon* **2018**, *131*, 201–212.
[30] a) H. Tan, R. Zhou, B. Zhang, *J. Power Sources* **2021**, *506*, 230179; b) Y. An, H. Fei, G. Zeng, L. Ci, B. Xi, S. Xiong, J. Feng, *J. Power Sources* **2018**, *378*, 66–72.
[31] X. Lin, J. Huang, B. Zhang, *Carbon* **2019**, *143*, 138–146.
[32] a) T. Placke, V. Siozios, R. Schmitz, S. Lux, P. Bieker, C. Colle, H.-W. Meyer, S. Passerini, M. Winter, *J. Power Sources* **2012**, *200*, 83–91; b) M. Winter, P. Novák, A. Monnier, *J. Electrochem. Soc.* **1998**, *145*, 428.
[33] Q. Liu, T. Zhang, C. Bindra, J. Fischer, J. Josefowicz, *J. Power Sources* **1997**, *68*, 287–290.
[34] N. Iwashita, C. R. Park, H. Fujimoto, M. Shiraishi, M. Inagaki, *Carbon* **2004**, *42*, 701–714.
[35] a) F. Bonhomme, J. Lassegues, L. Servant, *J. Electrochem. Soc.* **2001**, *148*, E450; b) F. Tuinstra, J. L. Koenig, *J. Chem. Phys.* **1970**, *53*, 1126–1130.
[36] L. Malard, M. A. Pimenta, G. Dresselhaus, M. Dresselhaus, *Phys. Rep.* **2009**, *473*, 51–87.
[37] A. Sadezky, H. Muckenhuber, H. Grothe, R. Niessner, U. Pöschl, *Carbon* **2005**, *43*, 1731–1742.
[38] a) M. Inagaki, F. Kang, *Materials Science and Engineering of Carbon: Fundamentals*, Butterworth-Heinemann (Elsevier), **2014**; b) M. Inagaki, A. Oberlin, T. Noda, *Tanso* **1975**, *1975*, 68–72.
[39] J. Maire, J. Mering, *Chem. Phys. Carbon* **1970**, *6*, 125–190.
[40] J. P. Olivier, M. Winter, *J. Power Sources* **2001**, *97*, 151–155.
[41] R. Nölle, K. Beltrop, F. Holtstiege, J. Kasnatscheew, T. Placke, M. Winter, *Mater. Today* **2020**, *32*, 131–146.
[42] L. Fan, Y. Hu, A. M. Rao, J. Zhou, Z. Hou, C. Wang, B. Lu, *Small Methods* **2021**, *5*, 2101131.
[43] L. Deng, Y. Zhang, R. Wang, M. Feng, X. Niu, L. Tan, Y. Zhu, *ACS Appl. Mater. Interfaces* **2019**, *11*, 22449–22456.
[44] W. Zhang, Z. Cao, W. Wang, E. Alhajji, A. H. Emwas, P. M. Costa, L. Cavallo, H. N. Alshareef, *Angew. Chem. Int. Ed.* **2020**, *59*, 4448–4455; *Angew. Chem.* **2020**, *132*, 4478–4485.
[45] D. Igarashi, K. Kubota, T. Hosaka, R. Tatara, T. Inose, Y. Ito, H. Inoue, M. Takeuchi, S. Komaba, *Electrochemistry* **2021**, 21–00062.
[46] a) J. Liu, T. Yin, B. Tian, B. Zhang, C. Qian, Z. Wang, L. Zhang, P. Liang, Z. Chen, J. Yan, X. Fan, J. Lin, X. Chen, Y. Huang, K. P. Loh, Z. X. Shen, *Adv. Energy Mater.* **2019**, *9*, 1900579; b) H. Onuma, K. Kubota, S. Muratsubaki, W. Ota, M. Shishkin, H. Sato, K. Yamashita, S. Yasuno, S. Komaba, *J. Mater. Chem. A* **2021**, *9*, 11187–11200.
[47] a) H. Buqa, R. Blyth, P. Golob, B. Evers, I. Schneider, M. S. Alvarez, F. Hofer, F. Netzer, M. Ramsey, M. Winter, *Ionics* **2000**, *6*, 172–179; b) Y.-P. Wu, E. Rahm, R. Holze, *J. Power Sources* **2003**, *114*, 228–236; c) H. Buqa, P. Golob, M. Winter, J. Besenhard, *J. Power Sources* **2001**, *97*, 122–125; d) R. I. R. Blyth, H. Buqa, F. P. Netzer, M. Ramsey, J. Besenhard, M. Winter, *J. Power Sources* **2001**, *97*, 171–173.
[48] T. Placke, S. Rothermel, O. Fromm, P. Meister, S. F. Lux, J. Huesker, H.-W. Meyer, M. Winter, *J. Electrochem. Soc.* **2013**, *160*, A1979.
[49] P. Meister, H. Jia, J. Li, R. Kloepsch, M. Winter, T. Placke, *Chem. Mater.* **2016**, *28*, 7203–7217.

Manuscript received: January 25, 2022
Revised manuscript received: February 20, 2022
Accepted manuscript online: February 22, 2022
Version of record online: March 9, 2022